Low-Voltage Fault Ride Through of the Modular Multilevel Converter in a Battery Energy Storage System Connected Directly to the Medium Voltage Grid

Low-Voltage Fault Ride Through of the Modular Multilevel Converter in a Battery Energy Storage System Connected Directly to the Medium Voltage Grid

A. Hillers and J. Biela
Laboratory for High Power Electronic Systems
ETH Zurich, Physikstrasse 3, CH-8092 Zurich, Switzerland
Email: hillers@hpe.ee.ethz.ch

***Abstract*—Nowadays, even small and medium sized power generators are required to ride through low-voltage faults without themselves from the grid. This presents a unique requirement to the modular multilevel converter (MMC) in a battery energy storage system based on split batteries (sBESS): In case of a low-voltage grid-fault, the arm voltages leave their steady-state trajectory which can lead to undervoltage or overvoltage in the arms, provoking an unacceptable shutdown of the whole converter. This paper presents a new control strategy to support the arm voltages by making use of the split batteries in case of fault. The converter can ride through consecutive grid-faults while supplying a short circuit current to support the grid and can immediately resume operation after the fault is cleared. Virtually no overdimensioning of the modules is needed and the system complies with fault-ride-through requirements of the transmission system operators.**

I. Introduction

With the increasing share of power-infeed from distributed generation, the European Network of Transmission System Operators for Electricity (ENTSO-E) is engaging also small and medium-sized generators in the static and dynamic grid stabilization. In case of a voltage sag, these generators may no longer disconnect themselves [1], and may be required to supply a short-circuit current [2].

For a split battery energy storage system (sBESS) based on the modular multilevel converter (MMC), this presents a unique requirement: In case of a low-voltage grid-fault, the arm voltages leave their steady-state trajectory, prospectively leading to undervoltages or overvoltages in the arms if the converter is not overdimensioned.

This paper proposes a new control methodology to overcome this limitation by using the split batteries to support the arm voltages during voltage sags in the power grid. Control schemes that fulfill similar requirements have been demonstrated for wind-turbines with doubly-fed induction generations [3] or full-power voltage source converters [4]. The converter is able to output a short circuit current to stabilize the power-grid. When the fault is cleared, the converter may immediately resume normal operation.

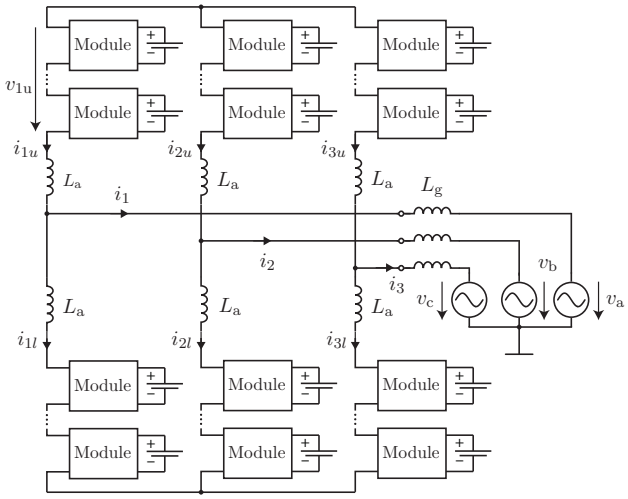

Fig. 1: Simplified circuit diagram of an energy storage system based on split batteries (sBESS). Each module has a battery attached to it.

Neither overdimensioning of the converter nor overdimensioning of the modules is required to achieve these goals. There is no recovery time, so consecutive grid-faults can be handled in the same way as one-off low-voltage sags.

To begin with, **Section II** briefly recapitulates the steady-state operation of the system when supplying power to a healthy grid and describes the role of the internal arm voltage in the modular multilevel converter. **Section III** introduces the fault ride-through requirements as imposed by the ENTSO-E and illustrates the problem of unwanted offsets on the internal arm voltage when the converter is recovering from voltage sags. In **section IV**, a simple and robust control methodology is proposed that uses the split batteries to support the arm voltage in these cases, allowing for a safe operation in all conditions. It is shown in **section VII**, that the influence on the design of the system is minimal. Finally, simulation results for a 20 kV, 5 MW system are shown in **section VI**.

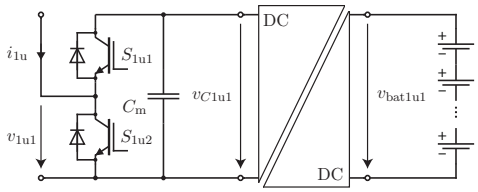

Fig. 2: Basic circuit diagram, exemplarily showing the first module in the upper arm of the first leg.

II. Operating Principles

The split battery energy storage system comprises a modular multilevel converter [5] with batteries integrated into the modules. Its basic circuit diagram is shown in Fig. 1. Bidirectional dc-dc converters decouple the power fluctuation within the arms from the charging process of the batteries to maximize their life time. A basic circuit diagram of a module is shown in Fig. 2. The converter has N modules per arm.

The inherent symmetry of the system allows for most considerations to be made exemplarily for the first leg, resp. the upper arm of the first leg resp. the first module within the upper arm of the first leg. This is adopted throughout this analysis wherever possible to prevent the excessive use of index variables. For the sake of readability, only the direction of power transfer to the grid is referred to in the text, even though all considerations are of course valid for both ways.

Under typical operating conditions, the voltages of all module capacitors in each arm are kept approximately equal. This is commonly achieved with the sorting algorithm discussed in [6]. The short-term average of the output voltage of each arm can thus in general be controlled to an arbitrary value v_{1u} between 0 V and the *internal arm voltage*

$$v_{1u,int} = \sum_{n=1}^{N} v_{C1un}, \tag{1}$$

and is typically regarded as continuous [7]. The total battery power

$$P_{1u,bat} = \sum_{n=1}^{N} P_{1un,bat}. \tag{2}$$

denotes the total power that all dc-dc converters together are feeding from the batteries into the arm. The internal arm energy

$$w_{1u,int} = \sum_{n=1}^{N} w_{C1un} = \sum_{n=1}^{N} \frac{1}{2} C_m v_{C1un} \tag{3}$$

is the sum of the energy in all module capacitors in one arm.

A. Steady-State Operation

In the following, the steady-state operation will be introduced on which the analysis of the fault-ride-through behavior is based. To simplify the calculations, it is assumed w.l.o.g., that the angle of the grid voltage is zero. Hence grid voltage V_g is real-valued.

The goal of the steady-state model is to calculate the a-priori unknown arm voltages v_{1u}, v_{1l}, v_{2u}, v_{2l}, v_{3u} and v_{3l}, by which the MMC can be controlled. These voltages are typically split into the parts $v_{1,line}$, $v_{2,line}$ and $v_{3,line}$ that only have an influence on the line-currents, and the parts $v_{1,circ}$, $v_{2,circ}$ and $v_{3,circ}$, that only influence the circulating currents [8]:

$$v_{1u} = \frac{V_{dc}}{2} - v_{1,line} + \underbrace{\frac{v_{1,circ}}{2}}_{\approx 0} \tag{4}$$

$$v_{1l} = \frac{V_{dc}}{2} + v_{1,line} + \underbrace{\frac{v_{1,circ}}{2}}_{\approx 0} \tag{5}$$

The part $v_{1,circ}$ is neglected through this analysis, because it is typically small compared to $v_{1,line}$. The circulating current itself is assumed to be controlled to zero.

In order to determine the arm voltages during-steady state, the voltage

$$v_{1,line} = \hat{V}_\alpha \cdot \cos(2\pi f t + \varphi_\alpha), \tag{6}$$

is calculated using common phasor arithmetics as shown in [9]:

$$\underline{i}_1 = \frac{\underline{S}}{3V_g}, \tag{7}$$

$$\hat{V}_\alpha = \sqrt{2}\left|\underline{i}_1 \cdot \left(\frac{j\omega L_a}{2} + j\omega L_g\right) + V_g\right|, \tag{8}$$

$$\varphi_\alpha = \angle\left(\underline{i}_1 \cdot \left(\frac{j\omega L_a}{2} + j\omega L_g\right) + V_g\right). \tag{9}$$

The variable $\underline{S}$ denotes the complex output power fed to the grid and $\omega = 2\pi f$ denotes the grid frequency. Because the arm voltages may not be negative, V_{dc} is chosen as follows

$$V_{dc} = 2\hat{V}_\alpha \cdot 1.15. \tag{10}$$

A margin of 15 % has been included for dynamic control. The arm current is:

$$i_{1u} = \frac{1}{2}\sqrt{2} I_1 \cos(\omega t + \varphi_i), \tag{11}$$

where $I_1 = |\underline{i}_1|$ and $\varphi_i = \angle \underline{i}_1$ are the RMS-value resp. the phase-angle of the output current.

B. Internal Arm Voltages

The fluctuation of the internal arm voltage is characteristic to the modular multilevel converter and presents an important design aspect. In order to ensure the safe operation of the converter, the internal arm voltages must always be kept within their designated boundaries. In the following it is explained, how the minimum and maximum value of the internal arm voltage influence the design of the converter.

The internal arm voltages are limited on the upper end by the maximum module voltage v_{crit}:

$$v_{1u,int,max} = N v_{crit}. \tag{12}$$

The maximum module voltage is typically determined by the critical voltage of the semiconductors. For the system considered in section VI, 4.5 kV switches are used, and $v_{\text{crit}} = 2.7\,\text{kV}$ has been chosen.

In addition, the internal module voltage must always be higher than the output voltage requirement of the respective arm. It is thus sufficient to chose

$$v_{\text{1u,int,min}} = V_{\text{dc}}. \tag{13}$$

Within these limits, the internal arm voltage may fluctuate. The cause of this fluctuation is the fluctuating arm power, which can be calculated from (11) and (6):

$$p_{\text{1u}} = \left(\frac{V_{\text{dc}}}{2} - \hat{V}_\alpha \cdot \cos(\omega t + \varphi_\alpha)\right) \frac{1}{2}\sqrt{2} I_1 \cos(\omega t + \varphi_i) \tag{14}$$

The total power fed into each arm also includes the total power fed from all batteries in the respective arm:

$$p_{\text{1u,tot}} = p_{\text{1u}} + P_{\text{1u,bat}} \tag{15}$$

The battery power $P_{\text{1u,bat}}$ is chosen such that the net energy transfer to the module capacitors is zero in steady-state:

$$P_{\text{1u,bat}} = \frac{\sqrt{2}}{4} I_1 \cdot \hat{V}_\alpha \cos(\varphi_i - \varphi_\alpha), \tag{16}$$

Because this value is constant in order to maximize the lifetime of the batteries, the total arm power (15) will fluctuate as well. This fluctuation is buffered by all module capacitors of the respective arm:

$$\begin{aligned} w_{\text{1u,int}} &= \int p_{\text{1u}} + P_{\text{1u,bat}}\,\mathrm{d}t \\ &= \frac{\sqrt{2} I_{\text{out}}}{4} \frac{2\sin(\omega t) V_{\text{dc}} - \hat{V}_\alpha \sin(2\omega t + \varphi_\alpha)}{\omega} + W_0, \end{aligned} \tag{17}$$

where $w_{\text{1u,int}}$ is the internal arm energy introduced in (3).

The minimum value $w_{\text{1u,int,min}}$ and the maximum value $w_{\text{1u,int,max}}$ of this fluctuation observed during the entire time of operation determine the size of the module capacitances as shown in [9]:

$$C_{\text{m}} \geq \frac{N \Delta w_{\text{1u}}}{v_{\text{crit}}^2 - (V_{\text{dc}} N)^2} = \frac{N(w_{\text{1u,int,max}} - w_{\text{1u,int,min}})}{v_{\text{crit}}^2 - (V_{\text{dc}} N)^2} \tag{18}$$

It is thus desired to keep the energy fluctuation to a minimum.

In the following, it is illustrated how $w_{\text{1u,int,min}}$ and $w_{\text{1u,int,max}}$ increase, when the converter is required to rides through a low voltage grid-fault without the dynamic support of the internal arm voltages. Afterwards, a control system is presented, that uses the split batteries to always keep the internal arm energies within the margin defined by the steady-state trajectory, eliminating the need to overdimension the module capacitances.

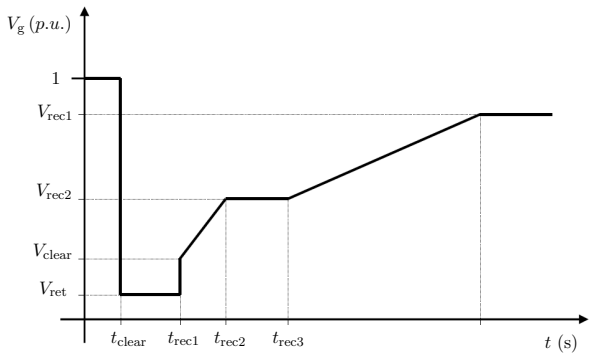

Fig. 3: Low-voltage fault ride-through requirements as published by the ENTSO-E for generators of *Type B*.

TABLE I: Voltage and time parameters for the fault tide through profile for generators of *Type B*.

Voltage Parameter	Value (p.u.)	Time Parameter	Value
V_{ret}	$0.05 - 0.15$	t_{clear}	$0.14\,\text{s} - 0.25\,\text{s}$
V_{clear}	$V_{\text{ret}} - 0.15$	t_{rec1}	t_{clear}
V_{rec1}	V_{clear}	t_{rec2}	$t_{\text{rec1}} - 0.7\,\text{s}$
V_{rec2}	0.85	t_{rec3}	$t_{\text{rec2}} - 1.5\,\text{s}$

III. Low Voltage Fault Ride Through

Nowadays, even small and medium sized grid-connected generators are required to ride through low-voltage faults without disconnecting. Fig. 3 shows the low-voltage fault ride-through profile for generators of *Type B*[1] as published by the ENTSO-E. As long as the grid voltage stays above this curve, the generator may not physically disconnect itself from the grid [1]. The voltage and time parameters can be chosen by the TSOs only within a limited range according to Tab. I. In addition, a TSO may require the generator to contribute to the short-circuit current to allow the installed protection equipment on the grid side to properly detect a fault [2].

For typical voltage source converters, the maximum short-circuit current is around 1 p.u. of the rated current [2]. Thus, it is assumed that the battery energy storage system may be required to contribute to the short circuit current of the grid by continuing to supply the nominal current during the voltage sag. In the following, it is shown how the internal arm voltages behave when they are not supported dynamically, as suggested in section IV.

A. Unsupported Fault Ride-Through

Fig. 4 shows the simulation results for a 5 MW, 20 kV sBESS riding through a sudden voltage sag down to a grid voltage of 0.1 p.u. while continuing to supply the nominal current. The internal arm voltages are not supported dynamically and thus leave their steady-state trajectory during the fault. Even though the power delivery from the batteries is adjusted to match the

[1] *Type B*: $\geq 1\,\text{MW}$ and $< 50\,\text{MW}$ in Continental Europe.

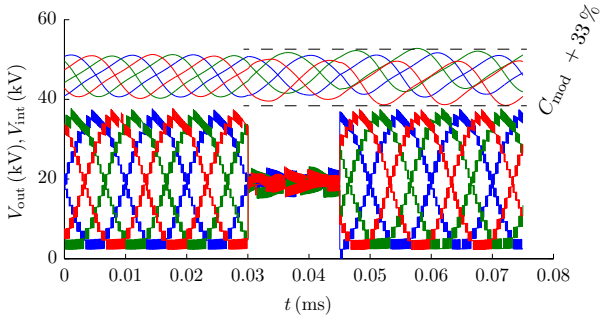

Fig. 4: Arm voltages and internal arm voltages during a voltage sag in the medium-voltage grid. When no corrective actions are taken, undervoltage and overvoltage occurs in the arms. **This figure will be redrawn before submission to the conference.**

new output power situation according to (16), the individual internal arm voltages will retain different offsets, when the voltage comes back.

In order to quantify this effect, the trajectories of the internal arm voltages have been calculated with the help of the steady-state model, by performing a parameter sweep over different fault times and different recovery times.

It was observed, that the arm voltages may end up with an offset of $+16\%$ or -16% in the worst case. Other voltage-vs-time profiles, that also fall under the requirements from the ENTSO-E, might lead to even worse situations.

To stay connected to the grid while continuing to deliver the nominal current without dynamic support of the arm voltages, the converter would according to (18) have to be designed with a module capacitance that is at least around 32% larger than the module capacitance required for safe operation in steady-state.

However, the split batteries present a degree of freedom, that has not yet been exploited: During the rare case of a voltage sag, the requirement to keep the power delivery from the batteries constant is weakened in favor of stabilizing the internal arm voltages. In the following, it is shown that the dc-dc converters that control the power delivery from the batteries do not have to be overdimensioned to achieve this. Afterwards, a complete control system is proposed, that can keep the arm voltages within the limits defined by the steady-state trajectory during a low voltage sag.

IV. Battery Support of the Arm Voltages

The goal of the battery support is to ensure that the arm voltage never leaves the boundaries defined by the steady-state trajectory. This way, the converter can be designed with minimum size of the module capacitances.

Two fundamental requirements are derived from this premise:

- First, the arm voltages may not leave these boundaries *during* a fault, and
- second, the arm voltages may not leave these boundaries *after* the fault.

While this formulation might seem redundant at a first glance, it expresses the different degrees of freedom available in both cases: When the voltage comes back while supplying a short circuit current I_{sc}, the converter will immediately continue to supply active power. For the case that $I_{\text{sc}} = I_{\text{nom}}$ this means that in order to satisfy (16), the dc-dc converters will already be operating at their maximum output power. Any correction of the steady-state trajectory that involves increasing the output power even further would increase the maximum power-rating of the dc-dc converter beyond the requirement for steady-state operation. This is not intended, and as shown in the next section, also not necessary. When the arm voltages are controlled to not deviate from the steady-state trajectory *during* the fault, they will also not retain an offset *after* the fault.

In the following, the theoretical considerations behind this approach are shown for the case that the converter is riding through the voltage sag shown in Fig. 4. Based on this, it is concluded that the converter can ride through any voltage sag of any magnitude, provided that the grid estimation and the control of the converter are sufficiently accurate and fast.

A. Power Requirements During A Fault

In the following, the total arm power required to fully support the arm voltages is calculated. This power is then taken as a reference in order to calculate the desired battery power, to actually achieve this. The total arm power that is required during a fault is calculated according to (14) and (15):

$$\widetilde{p}_{\text{1u,tot}} = \left(\frac{V_{\text{dc}}}{2} - \sqrt{\frac{2}{3}} V_{\text{g}} \cdot \cos(\omega t) \right) \frac{\sqrt{2} I_1}{2} \cos(\omega t + \varphi_i) + P_{\text{1u,bat}} \tag{19}$$

The voltage $\hat{\underline{V}}_\alpha$ and the phase angle φ_α have been approximated by the grid voltage $\sqrt{\frac{2}{3}} V_{\text{g}}$ and the grid phase angle $\varphi_{\text{g}} = 0$, which is according to (8) and (9) valid since L_{a} and L_{g} are reasonably small. The magnitude I_1 of the output current and the phase angle φ_i refers to the output current prior to the fault. The battery Power $\widetilde{P}_{\text{1u,bat}}$ is calculated according to (16):

$$\widetilde{P}_{\text{1u,bat}} = \frac{\sqrt{2}}{4} I_{\text{out}} \cdot \sqrt{\frac{2}{3}} V_{\text{g}} \cos(\varphi_i). \tag{20}$$

However, during a fault, the *actual* total arm power drops to:

$$p_{\text{1u,tot,fail}} = \left(\frac{V_{\text{dc}}}{2} - \sqrt{\frac{2}{3}} (1-a) V_{\text{g}} \cos(\omega t) \right) \frac{\sqrt{2} I_1}{2} \cos(\omega t + \varphi_i) + p^*_{\text{1u,bat,fail}} \tag{21}$$

The battery power $p^*_{\text{1u,bat,fail}}$ is no longer required to be constant and is determined later on. Again, the grid voltage and the phase angle of the grid are used as an approximation for the ideal control voltage $\hat{\underline{V}}_\alpha$ and the phase angle φ_α. The variable $a \in [0;1]$ denotes the magnitude, by which the grid

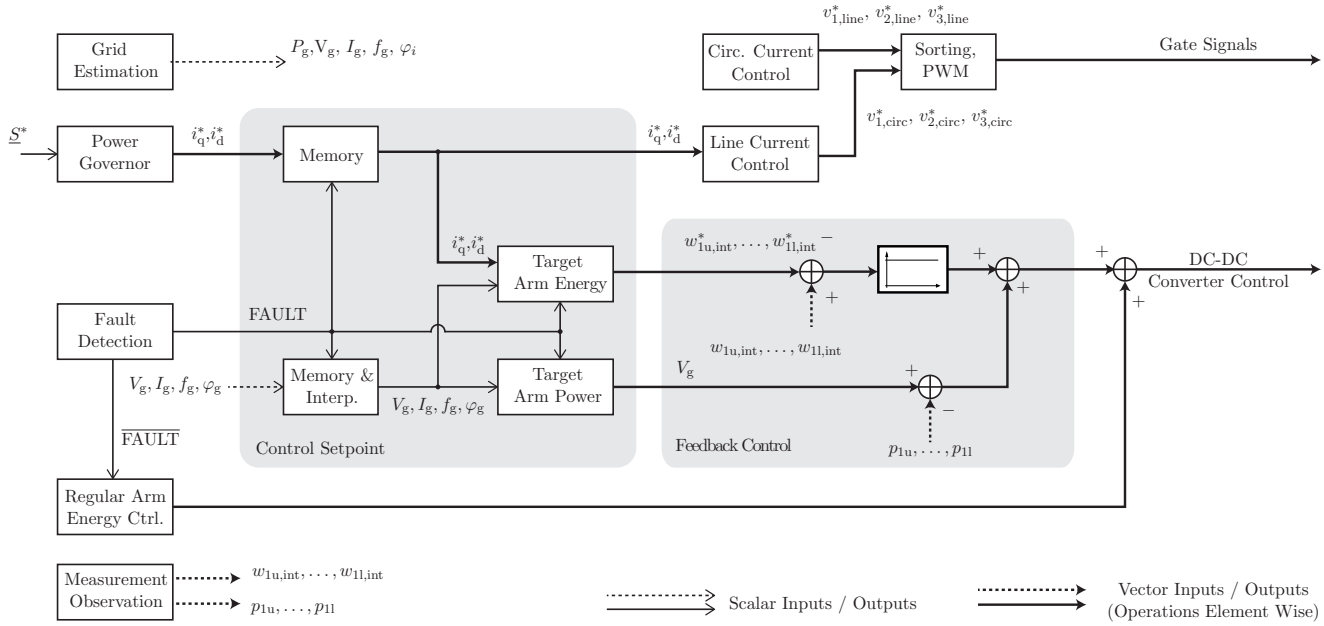

Fig. 5: Simplified control diagram of the modular multilevel converter used in the sBESS. The part, that belongs to the fault-ride-through control system, is shaded in grey. The remaining components represent a standard control system of the modular multilevel converter.

voltage drops. Because the grid can be expected to recover at any point in time, V_{dc} is kept constant at the value calculated in (10).

In order to achieve

$$p_{1u,tot,fail} = \widetilde{p}_{1u,tot}, \tag{22}$$

the total battery power thus needs to be:

$$p^*_{1u,bat} = -\frac{I_1 V_g}{2\sqrt{3}} \left(a\cos(\omega t)\cos(\omega t + \varphi_i) - \frac{\cos(\varphi_i)}{2} \right) \tag{23}$$

With the use of the trigonometric identity $\cos(a)\cos(b) = \cos(a+b)+\cos(a-b)$, this simplifies to

$$p^*_{1u,bat} = -\underbrace{\frac{I_1 V_g}{2\sqrt{3}}}_{\leq P_{1u,bat,nom}} \left[a\cos(2\omega t) + (a-1)\cos(\varphi_i) \right]. \tag{24}$$

It is now evident, that $p^*_{1u,bat}$ never exceeds $\frac{I_1 V_g}{2\sqrt{3}}$ because the absolute value of the term in the square brackets in (24) can never exceed one. Thus, the dc-dc converters can be designed with a nominal power of

$$P_{1u,bat,nom} = \frac{I_1 V_g}{2\sqrt{3}} \cdot 1.15, \tag{25}$$

which is under the assumptions made equal to the maximum power in steady-state already calculated in (16). A margin of 15 % for dynamic control has been added for the simulation shown in section VI. Moreover, the above is not only valid for the fault shown in (4), but suggests that any voltage profile like the one shown in Fig. 3, where a is a function of time, can be emulated this way.

However, (24) does *not* imply that the converter is in general able to emulate the steady-state trajectory for the operation with I_1 when the output current $I_{1,fail}$ during the fault is $I_{1,fail} < I_1$. This can be shown through replacing I_1 in (21) by $I_{1,fail}$, where $I_{1,fail} < I_1$. This has been omitted in this report for the sake of brevity.

An intuitive explanation can be found, by letting I_1 in (21) go to zero: Now, $p^*_{1u,bat}$ has to compensate for an increasing share of the whole power fluctuation $p_{1u,tot}$, which is far larger than the number calculated in (23). Another intuitive approach is to look at the part $\frac{I_1}{2}\frac{V_{dc}}{2}$, that was common to both operating modes, but now has to be compensated for as well.

While this might sound like a sever limitation at first, it merely implies, that the current can instantly be ramped down, but not instantly be ramped up during a fault. In fact, this is also typical to the regular operation of the modular multilevel converter. The same is true for quickly changing φ_i.

V. Control of The Arm Voltages in Case Of Fault

The theoretical considerations in section IV-A reveal how the converter can ride through a grid fault while keeping the internal arm energy within the boundaries defined by the steady-state trajectory.

A simple and robust control-scheme is proposed to achieve this. The control system is divided into the two main blocks highlighted in Fig. 5: The *Control Setpoint* subsystem calculates the target values for the total arm power and the internal arm energy. The *Feedback Control* subsystem then ensures that the internal arm voltages are accurately controlled to these

target values. In the following, both parts of the control system are discussed in detail.

A. Fault Detection and Control

Whenever a voltage sag is detected, the controller overrides the control command from the power-governor so that the converter can continue to supply the output current or an output current of reduced magnitude. This is denoted by the *Memory* block in Fig. 5 and the variables $\widetilde{i_\mathrm{d}}^*$ and $\widetilde{i_\mathrm{q}}^*$.

In addition to this, the converter needs a reference of the grid state, as it would have been, if no fault had happened. This is denoted by the *Memory & Interp.* block. In case of fault the variables $\widetilde{V}_\mathrm{g}$, $\widetilde{f}_\mathrm{g}$, and $\widetilde{f}_\mathrm{g}$ present an interpolation of the grid state, picking up from where it was right before the fault. This allows to calculate the target value of the total arm power during a fault:

$$\begin{aligned} p^*_{1\mathrm{u,tot}} = &\left(\frac{V_\mathrm{dc}}{2} - \underline{\hat{V}}_\alpha \cdot \cos(\omega t)\right)\frac{\sqrt{2}I_1}{2}\cos(\omega t + \varphi_i) \\ &+ \frac{\sqrt{2}}{4I_\mathrm{out}} \cdot \hat{V}_\alpha \cos(\varphi_i) \end{aligned} \tag{26}$$

The voltage $\underline{\hat{V}}_\alpha$ and phase-angle φ_α are calculated from the last known good grid state $\widetilde{V}_\mathrm{g}$, $\widetilde{f}_\mathrm{g}$ and the target currents $\widetilde{i_\mathrm{d}}^*$ and $\widetilde{i_\mathrm{q}}^*$ with the help of the equations discussed in section II-A.

The power needed from the batteries to support the internal arm voltages is calculated by subtracting the power $p_{1\mathrm{u}}$ from this target value:

$$p^*_{1\mathrm{u,bat}} = p_{1\mathrm{u}} - p^*_{1\mathrm{u,tot}} \tag{27}$$

The actual arm power $p_{1\mathrm{u}}$ can be measured indirectly, by measuring $i_{1\mathrm{u}}$ and $v_{1\mathrm{u}}$. The power $p_{1\mathrm{u,bat}}$ presents the setpoint for the total battery power $p_{1\mathrm{u,bat}}$ as shown in Fig. 5.

A feedback control is introduced in addition to the precontrol, that takes internal arm energy as a preference. The target value of the internal arm energy trajectory is calculated similar to the target value of the total arm power trajectory, based on the interpolated grid state:

$$\begin{aligned} w^*_{1\mathrm{u,int}} &= \int p^*_{1\mathrm{u,tot}}\,\mathrm{d}t \\ &= \frac{\sqrt{2}I_\mathrm{out}}{4}\frac{2\sin(\omega t)V_\mathrm{dc} - \hat{V}_\alpha \sin(2\omega t + \varphi_\alpha)}{\omega} + W_0 \end{aligned} \tag{28}$$

The voltage $\underline{\hat{V}}_\alpha$ and phase-angle φ_α are calculated the same way as before. The value of W_0 is adjusted so that it matches the offset of the actual trajectory before the fault occurred. The interpolated internal arm energy $w^*_{1\mathrm{u,int}}$ presents the reference, on which the feedback control acts. The control process can be implemented as a simple p-controller, because the plant itself is an integrator:

$$\Delta p^*_{1\mathrm{u,bat}} = k_\mathrm{p} \cdot (w^*_{1\mathrm{u,int}} - w_{1\mathrm{u,int}}) \tag{29}$$

The value $w_{1\mathrm{u,int}}$ can be measured indirectly by measuring the internal arm voltage. The complete plant is summarized again in the following equation:

$$w_{1\mathrm{u,int}} = \int p_{1\mathrm{u}} + p^*_{1\mathrm{u,bat}} + \Delta p^*_{1\mathrm{u,bat}}\,\mathrm{d}t \tag{30}$$

The remaining blocks of the control system are that of a typical MMC control system such as the ones discussed e.g. in [6] and [7]. The control of the arm-voltages in steady-state can be realized as shown in [10].

TABLE II: Specification of the presented sBESS.

Parameter		Value
Nominal Grid Voltage	V_g	20 kV
Nominal Grid Power	P_out	5 MW
Reactive Power	Q_out	$\pm 5\% P_\mathrm{out}$
Overall Battery Storage Capacity	W_tot	5 MWh
Number of modules per arm	N	20
Maximum module Voltage	V_crit	2.70 kV
Module Capacitance	C_m	690 μF
Arm Inductance	L_a	8 mH
Switching Frequency per Module	f_s	250 Hz

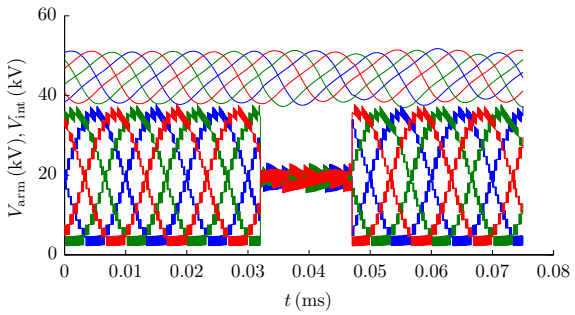

Fig. 6: Arm voltages and internal arm voltages during a voltage sag in the medium-voltage grid. With the proposed control scheme, the internal arm voltages follow their initial path, even in case of fault. **This figure will be redone before submission to the conference. An additional figure showing the output current will be included.**

VI. Simulation Results

In order to demonstrate the effectiveness of the proposed control-scheme, time-domain simulations have been performed for a 5 MW split battery energy storage system connected to the 20 kV distribution grid. The full specification of the system is given in Tab. II.

Fig. 6 shows the converter riding through the same fault as shown in Fig. 4, but this time, with the proposed control scheme enabled. Before the fault, the converter has been operating at the nominal current and continues to supply this current during and after the fault. The arm voltage always stays within the the limits defined by the steady-state trajectory and thus, the module capacitors do not have to be overdimensioned. The power-contribution from the batteries is shown in Fig. 7. It does not exceed the power-demand during steady-state, meaning that the dc-dc converter also do not need to be overdimensioned.

Even though, the theoretical considerations suggest that the difference in the trajectory of the internal arm voltage should

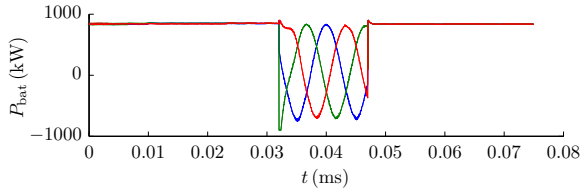

Fig. 7: Output power from the batteries riding through a low voltage sag.

not be visible, there is a slight change in trajectory. This is due to the fact, that prediction of the internal arm voltage does not completely match the systems actual behavior. It is thus even more important in a real system, that the parameters are accurately determined, and that the measurements are precise and fast.

The simulations already include a total control delay of $T_{\text{d}} = 25\,\mu$s between measurement of the grid-voltage and precontrol of the output voltage to account for the non-ideal nature of the real system.

VII. Influence in the Design of the sBESS

Without the support from the batteries during a voltage sag, the converter needs to be overdimensioned to cope with the larger voltage deviations in the module capacitances. Calculations for the voltage-drop depicted in Fig. 4 have shown, that the energy-fluctuation in the arms is in this case already increased by at least 32 %. According to (18), this leads to an increase of the module capacitance by the same factor.

When the converter is operated with the proposed control scheme, the arm voltages stay within their limits defined by the steady-state trajectory. Even though the batteries are used for the dynamical support, the dc-dc converter do not need to be overdimensioned, as the instantaneous battery power never exceeds the power-demand from the steady-state as shown in section IV-A

VIII. Conclusion

With the proposed control scheme, the split batteries can be beneficially used to support the arm voltages in case of fault. This way, a split battery energy storage system based on the modular multilevel converter is able to ride through a low voltage sag while continuing to supply a short-circuit current to the grid.

The proposed control scheme requires virtually no overdimensioning of the converter, and the system complies with the fault-ride through requirements of the the European Network of Transmission System Operators for Electricity (ENTSO-E).

The effectiveness of the proposed control is demonstrated by time-domain simulations for a 20 kV, 5 MW split battery energy storage system (sBESS) directly connected to the medium-voltage grid.

In contrast to that, it has been shown that in case of a typical grid-fault with a voltage drop down to 0.1 p.u., the overdimensioning of the module capacitors may be as large as 32 % for a converter where the arm voltages are not dynamically supported. Thus, the proposed control system prohibits an increases of both the costs and the volume of the system, since the module capacitors are typically by far the largest passive components in the MMC.

Acknowledgment

The authors would like to thank *ABB Switzerland Ltd.* and the *Bundesamt fur Energie* (BFE) for their financial support of this very interesting project.

References

[1] ENTSO-E, "Network code for requirements for grid connection applicable to all generators," Online, ENTSO-E, June 2012.

[2] BDEW, "Technische richtlinie erzeugungsanlage am mittelspannungsnetz," Online, BDEW, June 2008.

[3] M. Rathi and N. Mohan, "A novel robust low voltage and fault ride through for wind turbine application operating in weak grids," in *Annual Conference of IEEE Industrial Electronics Society (IECON)*, Nov. 2005.

[4] Y. Chen, Y. Yang, L. Wang, and W. Wu, "A low voltage ride-through control strategy of full power converter wind turbine system under balance grid fault," in *International Conference on Electrical Machines and Systems (ICEMS)*, Aug. 2011, pp. 1–6.

[5] J. H. R. Marquardt, A. Lesnicar, "Modulares Stromrichterkonzept fur Netzkupplungsanwendung bei hohen Spannungen," in *ETG-Fachtagung, Bad Nauheim, Germany*, 2002.

[6] D. Siemaszko, A. Antonopoulos, K. Ilves, M. Vasiladiotis, L. Aandngquist, and H.-P. Nee, "Evaluation of control and modulation methods for modular multilevel converters," in *International Power Electronics Conference (IPEC)*, June 2010, pp. 746–753.

[7] A. Antonopoulos, L. Angquist, and H.-P. Nee, "On dynamics and voltage control of the modular multilevel converter," in *European Conference on Power Electronics and Applications (EPE)*, Sept. 2009, pp. 1–10.

[8] S. Norrga, L. Angquist, K. Ilves, L. Harnefors, and H.-P. Nee, "Decoupled steady-state model of the modular multilevel converter with half-bridge cells," in *IET International Conference on Power Electronics, Machines and Drives (PEMD)*, Mar. 2012, pp. 1–6.

[9] A. Hillers and J. Biela, "Optimal design of the modular multilevel converter for an energy storage system based on split batteries," in *European Conference on Power Electronics and Applications (EPE)*, Sept. 2013.

[10] A. Hillers and J. Biela, "Fault-tolerant operation of the modular multilevel converter in an energy storage system basedbd on split batteries," in *European Conference on Power Electronics and Applications (EPE)*, Aug. 2014.